Supporting Information

Bothma et al. 10.1073/pnas.1410022111

SI Text

SI Methods

Cloning and Transgenesis. A plasmid construct containing the *even-skipped* (*eve*) enhancer and promoter region (−1.7 kb, +50 bp) was built using the pbPHi backbone vector containing *yellow* reporter gene (1, 2). The *yellow* reporter gene (6.4 kb) was used instead of *lacZ* (5.3 kb) (3) to increase the signal strength, which is proportional to the length of the reporter. This is because the number of transcripts associated with the template is directly proportional to the length of the reporter when the MS2 repeats are placed in the 5′ position. Primers used for building the construct are atttgcggccgcCAAGAAGGCTTGCATGTGGG and cgggatccAACGAAGGCAGTTAGTTGTTGACTG. Copies of the MS2 stem loops were extracted from plasmid pCR4-24XMS2SL-stable (Addgene; 31865) by digesting it with BamHI and BglII restriction enzymes. This fragment was ligated into *eve-yellow* pbPHI vector linearized with BamHI. The *eve2*-MS2-yellow plasmid was integrated on chromosome 3 (Vk33).

In Situ Hybridization and Fluorescence Microscopy. Fluorescent in situ hybridization was performed as described previously using hapten-tagged complementary mRNA probes (4, 5). Embryos were imaged on a Zeiss 700 laser-scanning microscope in *z* stacks through the nuclear layer at 0.5-μm intervals using a Plan-Apochromat 20×/0.8 air lens.

Live Imaging Sample Preparation and Data Acquisition. Female virgins of line yw; Histone-RFP;MCP-NoNLS-GFP (3) were crossed with males of the reporter line (*eve2*-MS2-yellow). Collected embryos were dechorinated with bleach and mounted between a semipermeable membrane (Biofolie; In Vitro Systems & Services) and a coverslip and embedded in Halocarbon 27 oil (Sigma). Excess oil was removed with absorbent paper from the sides to flatten the embryos slightly. The flattening of the embryos makes it possible to image more nuclei in the same focal plane without causing any detectable change to early development processes (6).

Embryos were either imaged using a custom-built two-photon microscope (7) at Princeton and a Zeiss LSM 780 confocal microscope at University of California, Berkeley. On the two-photon microscope, imaging conditions were as described by Garcia et al. (3): average laser power at the specimen was 10 mW, a pixel size is 220 nm, and image resolution is 512 × 256 pixels. At each time point, a stack of 10 images separated by 1 μm was acquired, resulting in a final time resolution of 37 s. Confocal imaging on the Zeiss LSM 780 was performed using a Plan-Apochromat 40×/1.4 N.A. oil immersion objective. The MCP-GFP and Histone-RFP were excited with a laser wavelength of 488 and 561 nm, respectively. Fluorescence was detected with two separate photomultiplier tubes using the Zeiss QUASAR detection unit (gallium–arsenide–phosphide photomultiplier was used for the GFP signal, whereas the conventional detector was used for the RFP). Pixel size is 198 nm, and images were captured at 512 × 512 pixel resolution with the pinhole set to a diameter of 116 μm. At each time point, a stack of 22 images separated by 0.5 μm were captured, spanning the nuclear layer. The final time resolution is 32 s.

Live-Imaging Data Analysis. Analysis was performed as described in ref. 3. Histone-RFP slices were maximum projected for each time point. Nuclei were segmented using a blob detection approach based on the Laplacian of Gaussian filter kernel. The segmented nuclei were then tracked over multiple nuclear cycles. Initially, each time frame of the MCP-GFP channel is treated independently. Spots are detected in 3D using raw images and assigned to their respectively closest nucleus. When multiple spots are detected in the vicinity of the nucleus (due to segregating sister chromatids), only the brightest one is kept. When single traces are shown, the automated tracking of both nuclei and spots was checked manually frame by frame using custom analysis code. Spot intensity determination requires an estimate of the local fluorescent background for each particle. Two-dimensional Gaussian fits to the peak plane of each particle column determines an offset, which is used as background estimator. The intensity is calculated by integrating the particle fluorescence over a circle with a radius of 6 pixels and subtracting the estimated background. Imaging error is dominated by the error made in the fluorescent background estimation (3).

In ref. 3, it was possible to measure the average fluorescence per polymerase molecule for the *hunchback*>MS2 transgene with 24 MS2 repeats. The quantitative imaging for the *eve*>MS2 transgene was conducted under the exact same imaging conditions on the same microscope. The *eve*>MS2 transgene also possess 24 MS2 repeats. However, the specific sequence of the stem loops is slightly different as these repeats have been further optimized to facilitate molecular biology work with them (8). Assuming that the MS2 sites are similarly saturated in both cases, we can then use the average fluorescence per polymerase molecule calculated for the *hunchback*>MS2 transgene to calibrate the *eve*>MS2 fluorescent traces in terms of the absolute number of transcribing polymerases per fluorescent spot (Fig. 4). It is important, however, to point out that this is an estimate and that a direct calibration between fluorescence and MS2-*eve* transcripts will be necessary for further confidence.

We quantified expression domain refinement dynamics by fitting a Gaussian curve to the profile of the fraction of active nuclei as a function of anterior-posterior (AP) position at each time point in nuclear cycle 14 (nc14) (Fig. 2*D*, dashed line). The fits define an expression domain width over which we determined the instantaneous fraction of active nuclei. The width of the expression domain as well as the fraction of active nuclei refine into the mature stripe pattern during the initial 20 min of expression (Fig. 2*E*).

Determining the Amount of mRNA Accumulated in the Presence of Degradation. In the experiments reported here, the quantity that is measured is the observed fluorescence in foci of transcription, which is proportional to the number of nascent mRNA molecules associated with a locus at a specific time. This is related to, but not exactly equal to, the rate of mRNA production. One quantity that is of particular interest is how much mRNA has accumulated in individual cells at a specific time point. To connect the measured fluorescence to the amount of mRNA produced by a cell up to a given time, we have to obtain the rate of mRNA production from the fluorescence traces and then account for the corresponding mRNA degradation. In the following sections, we give details on how this magnitude is calculated. The first section describes how to connect the measured fluorescence with the rate of mRNA production, and the second describes how we to use the obtained mRNA production rate to estimate the amount of accumulated mRNA in the presence of degradation.

Relating Measured Fluorescence to mRNA Production Rate. The observed fluorescence in foci of transcription as a function of time is given by $F(t)$. This quantity is linearly related to the number of mRNA molecules associated with the DNA template at a given instant. In our model, mRNA molecules remain associated with the DNA template for as long as it takes the transcribing polymerase to traverse the length of the gene, E_t. Hence, after a time $(E_t + t)$, all of the mRNA associated with the active locus at a time t have been released from the template. Thus,

$$F(t) = \overline{N_p}(t + E_t) - \overline{N_p}(t),$$

where $\overline{N_p}(t)$ is the number of mRNAs that have been produced up to time point t, properly scaled by the average fluorescence intensity for a single mRNA molecule. Now, we can expand $\overline{N_p}(t + E_t)$ around $E_t/2$, which results in the following:

$$\overline{N_p}(t + E_t) = \overline{N_p}\left(t + \frac{E_t}{2} + \frac{E_t}{2}\right) = \sum_{n=0}^{\infty} \frac{\overline{N_p}^{(n)}\left(t + \frac{E_t}{2}\right)}{n!}\left(\frac{E_t}{2}\right)^n.$$

Similarly, we can expand $\overline{N_p}(t)$, obtaining the following:

$$\overline{N_p}(t) = \overline{N_p}\left(t + \frac{E_t}{2} - \frac{E_t}{2}\right) = \sum_{n=0}^{\infty} \frac{\overline{N_p}^{(n)}\left(t + \frac{E_t}{2}\right)}{n!}\left(-\frac{E_t}{2}\right)^n.$$

As a result,

$$\overline{N_p}(t + E_t) - \overline{N_p}(t) = \sum_{n=0}^{\infty} \frac{\overline{N_p}^{(2n+1)}\left(t + \frac{E_t}{2}\right)}{(2n+1)!}\left(\frac{E_t}{2}\right)^{2n+1}$$

$$= \frac{d\overline{N_p}}{dt}\left(t + \frac{E_t}{2}\right) \times \left(\frac{E_t}{2}\right) + \text{h.o.t},$$

where "h.o.t" indicates higher-order terms. This implies that

$$F(t) \approx \frac{d\overline{N_p}}{dt}\left(t + \frac{E_t}{2}\right) \times \left(\frac{E_t}{2}\right)$$

and

$$\frac{d\overline{N_p}(t)}{dt} \approx \frac{2}{E_t} \times F\left(t - \frac{E_t}{2}\right).$$

As a result, by integrating the measured fluorescence one can obtain, up to a multiplicative constant, the amount of mRNA produced as a function of time. The details on how this is done is detailed in the next section.

Relating mRNA Production Rate to Amount of mRNA Accumulated. In the previous section, we derived a connection between the measured fluorescence and the rate of mRNA production. In the absence of mRNA degradation and neglecting diffusion of mRNA between cells, the total amount of mRNA associated with a given nucleus at a given time is as follows:

$$\overline{N_{\text{mRNA}}}(t) = \int_0^t \frac{d\overline{N_p}(\tau)}{dt} d\tau.$$

If we have to allow for mRNA degradation according to first-order kinetics, this simply becomes the following:

$$\overline{N_{\text{mRNA}}}(t) = \int_0^t \left(\frac{d\overline{N_p}(\tau)}{dt} - \lambda \times \overline{N_{\text{mRNA}}}(\tau)\right) d\tau.$$

Hence, given some initial conditions and the rate of mRNA production estimated from our measurements, we can integrate the above equation to obtain the accumulated amount of mRNA present in a cell at a given time.

SI Discussion

Using the methods explained in the previous sections, it is possible to relate the measured fluorescence (Fig. S1*A*) to the amount of mRNA accumulated (Fig. S1*B*). Fig. S1*B* shows how the amount of accumulated mRNA changes with time when one assumes different half-lives. When the mRNA half-life is short, the accumulated amount of mRNA plateaus relatively soon into cell cycle 14 while it steadily increases with time for longer half-lives. The overall levels of mRNA accumulated also scales with the mRNA half-life. One of the things we wanted to get a sense of is how different half-lives of mRNA affect the qualitative profile of the stipe. To look at this, we determined the mRNA accumulation profile for a given embryo assuming different half-lives (Fig. S1 *C* and *D*, and Movie S5). Although there appears to be a modest increase in the width of the stripe as the mRNA half-life is increased, it is not a striking difference. Fig. S1*E* shows that increasing the mRNA half-life from 5 to 60 min only leads to a small increase in the number of cells on the boundary of the stripe even though the half-life is varied by more than an order of magnitude. Movie S5 does show how the persistence of mRNA increases as the mRNA half-life is increased. It is not clear how biologically relevant the persistence of the mRNA driven by stripe 2 enhancer is later because there is an autoregulatory enhancer that takes over from the eve 2 enhancer to drive expression later (9).

In this study, we have looked at the dynamics of mRNA accumulation. How this will connect to the dynamics of the protein distribution will depend strongly on the half-life of the eve protein in the early embryo. Although this has not been measured for eve, the half-lives of the ftz and engrailed proteins have been measured and both found to be short, <10 min (10, 11). Hence it is likely that the eve protein will have a lifetime on this order [also consistent with estimates from modeling work (12)]. With such a short half-life, the evolution of the protein pattern will be closely coupled to that of the accumulated mRNA pattern.

We relate the fluorescence dynamics to the rate of RNA polymerase II (Pol II) loading at the promoter by invoking a simple model previously used to analyze the mean transcriptional activity of multiple MS2 spots (3). In the following section, we describe the general idea of the models, how they are used to fit the data and extract the single-cell dynamics of transcriptional initiation.

A cartoon depicting one possible outcome in the context of a two-state promoter is shown in Fig. 4 *B–D*. Here, at time t_1 after mitosis Pol II molecules are loaded at a constant rate r. Because at this point in time the gene is devoid of Pol II molecules, the fluorescence will increase as more polymerases escape the promoter and are loaded onto the gene. If the transcriptionally active state persists for a time longer than the time required for the first Pol II molecule to reach the end of the gene [6.4 kbp, which take 4.2 ± 0.4 min to transcribe (3)], the number of Pol II molecules on the gene will reach steady state, resulting in a constant fluorescence signal. At time t_2, the promoter switches back to the OFF state and Pol II molecules are not further loaded at the promoter while those that have finished elongation fall off the gene, resulting in a steady decrease of fluorescence intensity. This whole process can be repeated with

different characteristic times resulting in the modulation of the burst size and frequency.

In a "multistate" transcription model (Fig. 4 *B–D*), the promoter can load Pol II molecules onto the gene a varying discrete rates. The result is more complex fluorescence dynamics, but the connection between the fluorescent signal and the rate of transcriptional initiation remains the same as in the case of the "two-state" transcription model.

Fits of the model to the fluorescence data to extract the dynamics of transcriptional initiation were performed manually using custom-written code in Matlab. It is important to point out that these fits should only be seen as an estimate of the dynamics. An unbiased algorithm to fit the data in an automated way is currently under development and will allow for the systematic characterization of these in vivo single-molecule data.

1. Venken KJT, He Y, Hoskins RA, Bellen HJ (2006) P[acman]: A BAC transgenic platform for targeted insertion of large DNA fragments in *D. melanogaster*. *Science* 314(5806): 1747–1751.
2. Perry MW, Boettiger AN, Bothma JP, Levine M (2010) Shadow enhancers foster robustness of *Drosophila* gastrulation. *Curr Biol* 20(17):1562–1567.
3. Garcia HG, Tikhonov M, Lin A, Gregor T (2013) Quantitative imaging of transcription in living *Drosophila* embryos links polymerase activity to patterning. *Curr Biol* 23(21): 2140–2145.
4. Bothma JP, Magliocco J, Levine M (2011) The snail repressor inhibits release, not elongation, of paused Pol II in the *Drosophila* embryo. *Curr Biol* 21(18):1571–1577.
5. Kosman D, et al. (2004) Multiplex detection of RNA expression in *Drosophila* embryos. *Science* 305(5685):846.
6. Di Talia S, Wieschaus EF (2012) Short-term integration of Cdc25 dynamics controls mitotic entry during *Drosophila* gastrulation. *Dev Cell* 22(4):763–774.
7. Liu F, Morrison AH, Gregor T (2013) Dynamic interpretation of maternal inputs by the *Drosophila* segmentation gene network. *Proc Natl Acad Sci USA* 110(17):6724–6729.
8. Hocine S, Raymond P, Zenklusen D, Chao JA, Singer RH (2013) Single-molecule analysis of gene expression using two-color RNA labeling in live yeast. *Nat Methods* 10(2): 119–121.
9. Harding K, Hoey T, Warrior R, Levine M (1989) Autoregulatory and gap gene response elements of the *even-skipped* promoter of *Drosophila*. *EMBO J* 8(4):1205–1212.
10. Edgar BA, Odell GM, Schubiger G (1987) Cytoarchitecture and the patterning of *fushi tarazu* expression in the *Drosophila* blastoderm. *Genes Dev* 1(10):1226–1237.
11. Kellerman KA, Mattson DM, Duncan I (1990) Mutations affecting the stability of the *fushi tarazu* protein of *Drosophila*. *Genes Dev* 4(11):1936–1950.
12. Jaeger J, et al. (2004) Dynamic control of positional information in the early *Drosophila* embryo. *Nature* 430(6997):368–371.

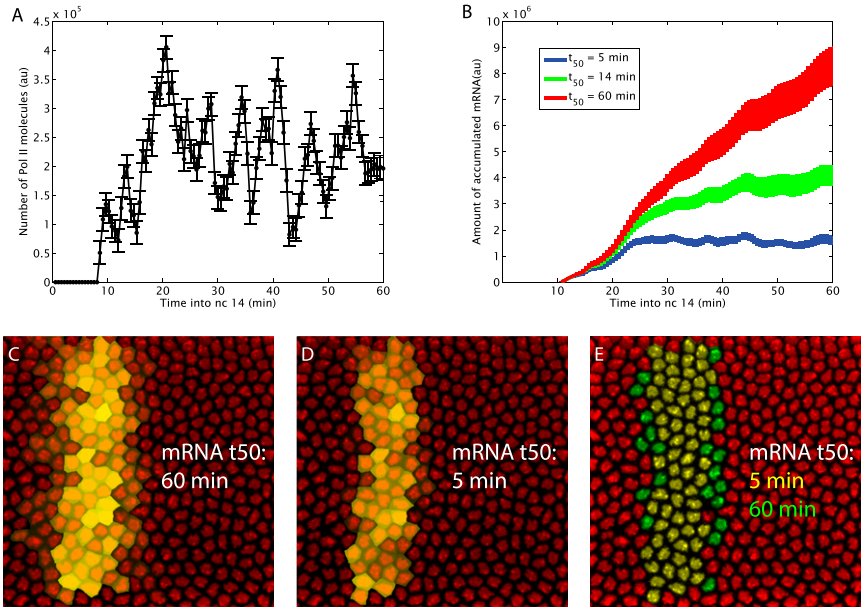

Fig. S1. Role of mRNA half-life on mRNA accumulation and profile of the stripe domain. (*A*) Fluorescence intensity as a function of time for an individual spot in the center of the *eve* expression pattern. (*B*) Calculated accumulated mRNA as a function of time for different mRNA half-lives. (*C* and *D*) Profile of the accumulated mRNA in an embryo when different half-lives are assumed, the false coloring of nuclei indicating the amount of mRNA produced. Each panel has been rescaled according to the maximum amount of mRNA accumulated during the course of the movie. (*E*) False-colored nuclei showing the stripe domain for 5- and 60-min half-lives. Nuclei were chosen to be within the stripe domain if they had an accumulated mRNA amount that was at least 25% of the maximum amount accumulated. [*A*, Error bars are imaging errors as in Garcia et al. (3); *B*, error bars are propagated from *A*; *C*, error bars correspond to the SEM over four embryos.]

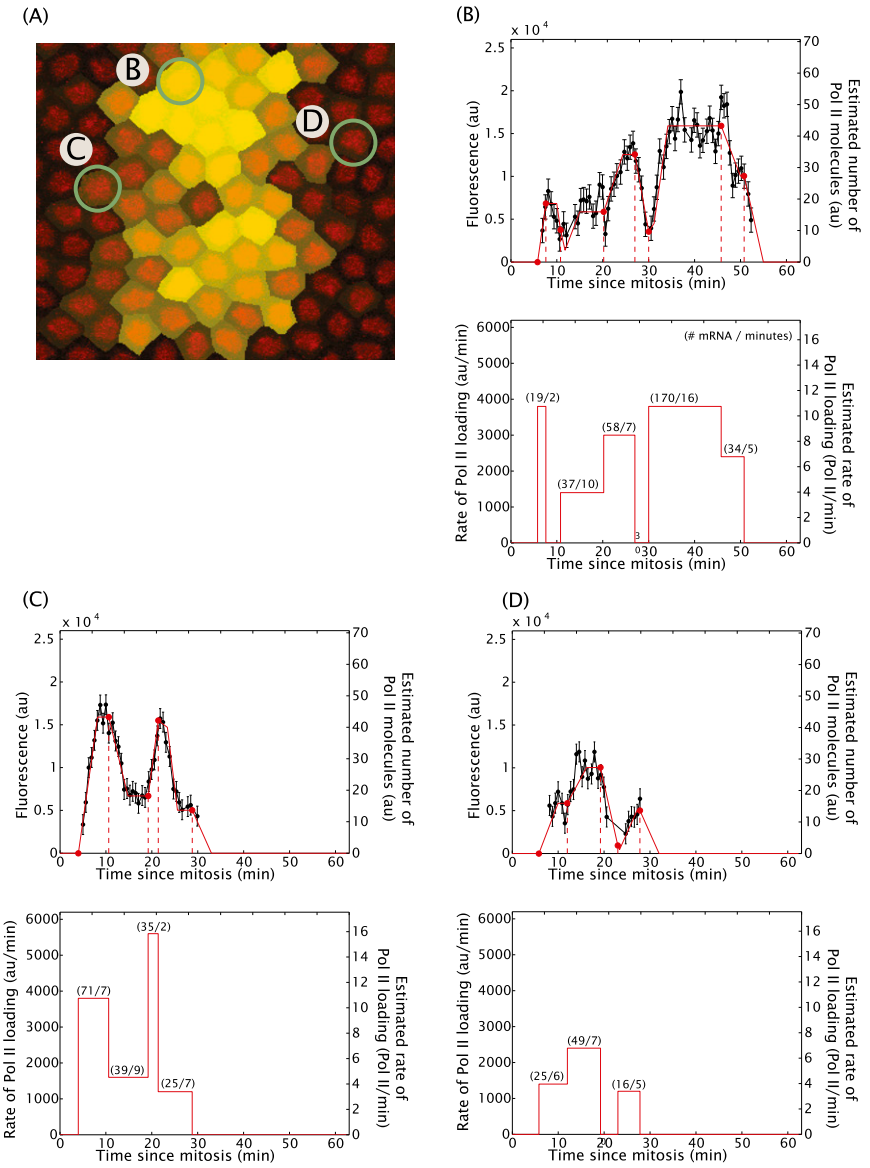

Fig. S2. Further evidence of transcriptional bursting in the *eve* stripe 2 domain. False coloring of nuclei indicating the amount of mRNA produced (Fig. 2 *D–F*). (*B–D*) Fluorescence intensity as a function of time for individual spots corresponding to the nuclei shown in *A* and estimated rate of Pol II loading resulting from manual fits as in Fig. 4. Note that transitions between multiple discrete states of transcription can be seen both inside and outside the mature stipe. The estimated number of mRNA molecules produced per state and their duration are shown. [Error bars are imaging errors as in Garcia et al. (3).]

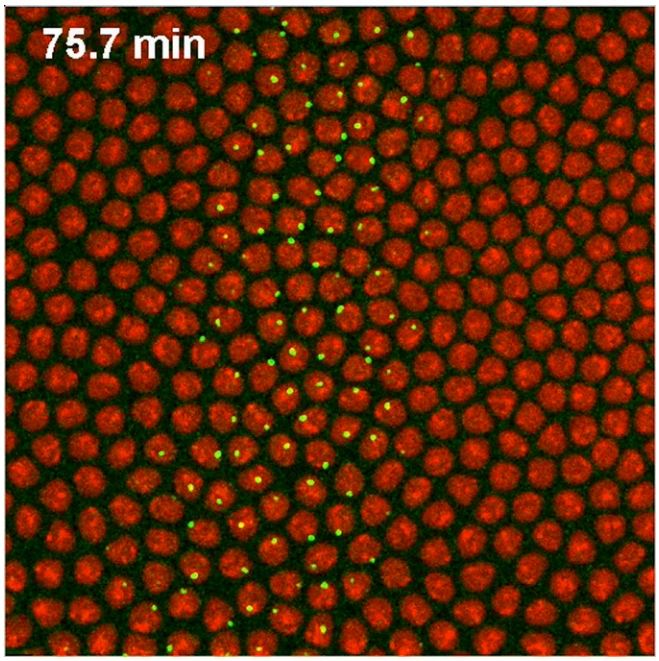

Movie S1. Dynamics of *eve* stripe 2 expression. Maximum projection of *eve*>MS2 transgene from nc11 to nc14 over 112 μm × 112-μm region centered on the stripe. Anterior is to the *Left*. The pattern is initially broad and gets refined during successive cell cycles to later on disappear at the onset of gastrulation. The snapshots from Fig. 1 are taken from this movie.

Movie S1

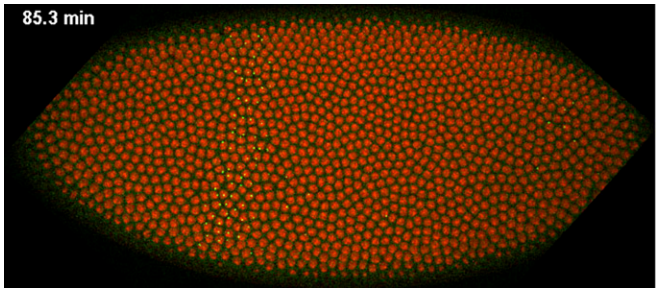

Movie S2. Whole-embryo dynamics of *eve* stripe 2 expression. Maximum projection of *eve*>MS2 transgene from end of nc10 to gastrulation for a whole embryo. Anterior is to the *Left*.

Movie S2

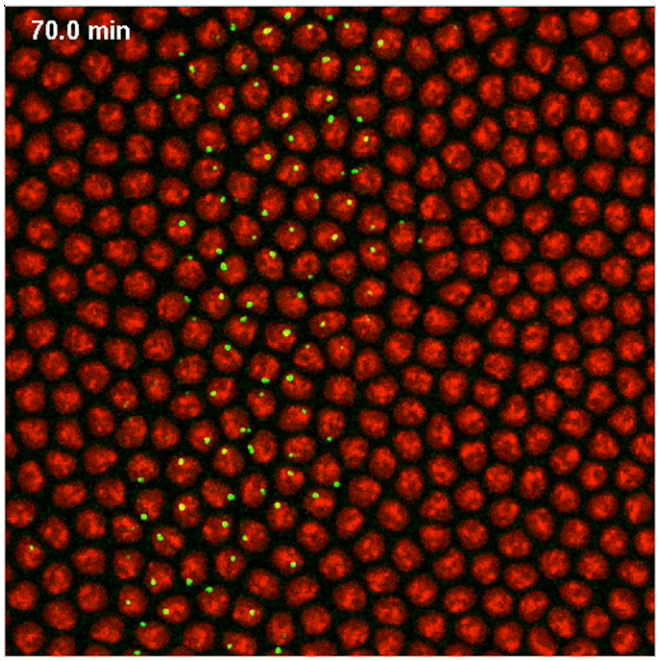

Movie S3. Further example of dynamics of *eve* stripe 2 formation. Maximum projection of *eve*>MS2 transgene from nc12 to nc14 over 112 μm × 112-μm region centered on the stripe. Anterior is to the *Left*. The pattern is initially broad and then gets refined during successive cell cycles and then the pattern eventually disappears.

Movie S3

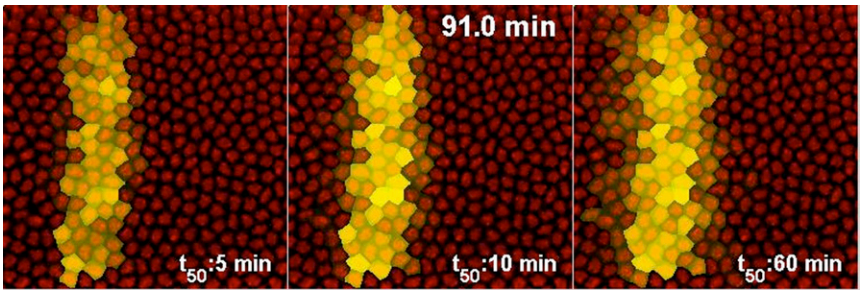

Movie S4. Effect of mRNA degradation on stripe formation. mRNA accumulation in the presence of degradation. The accumulated amount of mRNA per cell is shown as a function of time assuming different mRNA half-lives. The amount of accumulated mRNA is proportional to the degree of yellow false coloring. Because the absolute amount of mRNA accumulated is very different for different half-lives, each panel has been scaled according to the maximum accumulation reached during the course of each movie.

Movie S4

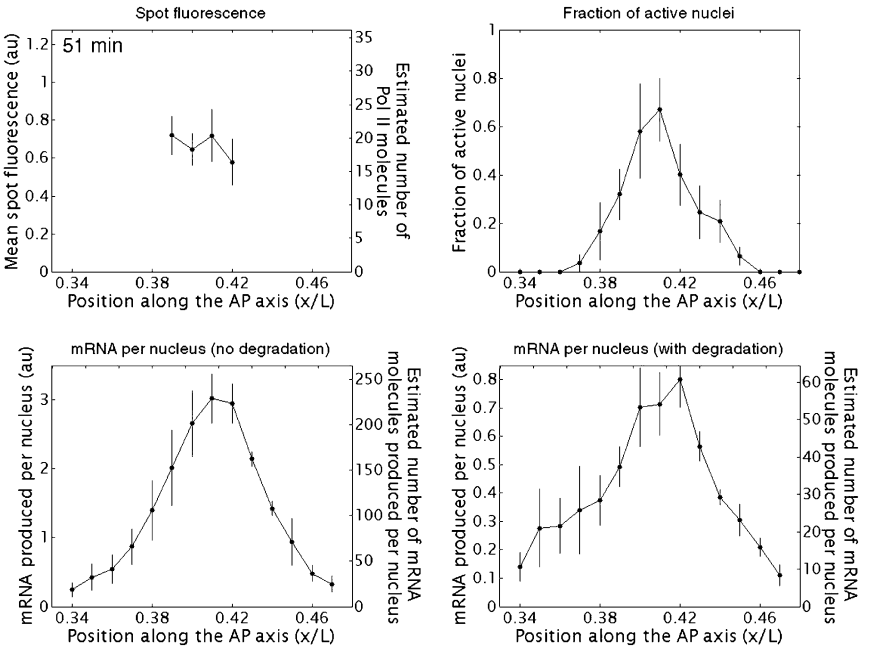

Movie S5. Quantitative dynamics of stripe formation and refinement. The mean spot fluorescence, instantaneous fraction of active nuclei, and accumulated amount of mRNA produced as a function of AP position are shown for different time points as in Fig. 3. The time stamp indicates time since the beginning of nc14. The mRNA produced us shown in the case of infinite half-life (mRNA accumulation) and of a half-life of 7 min. All data are obtained by averaging four different embryos. Error bars are SEM.

Movie S5